arXiv:astro-ph/0302220v2 25 Jun 2003

Accepted by the *Astrophysical Journal*

First Year *Wilkinson Microwave Anisotropy Probe* (*WMAP*[1]) Observations: Interpretation of the TT and TE Angular Power Spectrum Peaks

L. Page[2], M. R. Nolta[2], C. Barnes[2], C. L. Bennett[3], M. Halpern[4], G. Hinshaw[3], N. Jarosik[2], A. Kogut[3], M. Limon[3,9], S. S. Meyer[5], H. V. Peiris[6], D. N. Spergel[6], G. S. Tucker[7,9], E. Wollack[3], E. L. Wright[8]

page@princeton.edu

ABSTRACT

The CMB has distinct peaks in both its temperature angular power spectrum (TT) and temperature-polarization cross-power spectrum (TE). From the *WMAP* data we find the first peak in the temperature spectrum at $\ell = 220.1 \pm 0.8$ with an amplitude of $74.7 \pm 0.5\,\mu$K; the first trough at $\ell = 411.7 \pm 3.5$ with an amplitude of $41.0 \pm 0.5\,\mu$K; and the second peak at $\ell = 546 \pm 10$ with an amplitude of $48.8 \pm 0.9\,\mu$K. The TE spectrum has an antipeak at $\ell = 137 \pm 9$ with a cross-power of $-35 \pm 9\,\mu\mathrm{K}^2$, and a peak at $\ell = 329 \pm 19$ with cross-power $105 \pm 18\,\mu\mathrm{K}^2$. All uncertainties are 1σ and include calibration and beam errors.

An intuition for how the data determine the cosmological parameters may be gained by limiting one's attention to a subset of parameters and their effects on the peak characteristics. We interpret the peaks in the context of a flat adiabatic ΛCDM model with the goal of showing how the cosmic baryon density, $\Omega_b h^2$, matter density, $\Omega_m h^2$, scalar index, n_s, and age of the universe are encoded in their positions and amplitudes. To this end, we introduce a new scaling relation for the TE antipeak-to-peak amplitude ratio and recompute known related scaling relations for the TT spectrum in light of

[1] *WMAP* is the result of a partnership between Princeton University and the *NASA* Goddard Space Flight Center. Scientific guidance is provided by the *WMAP* Science Team.

[2] Dept. of Physics, Princeton University, Jadwin Hall, Princeton, NJ 08544

[3] Code 685, Goddard Space Flight Center, Greenbelt, MD 20771

[4] Dept. of Physics and Astronomy, University of British Columbia, Vancouver, BC Canada V6T 1Z1

[5] Depts. of Astrophysics and Physics, EFI and CfCP, University of Chicago, Chicago, IL 60637

[6] Dept. of Astrophysical Sciences, Princeton University, Princeton, NJ 08544

[7] Dept. of Physics, Brown University, Providence, RI 02912

[8] UCLA Astronomy, PO Box 951562, Los Angeles, CA 90095-1562

[9] National Research Council (NRC) Fellow

the *WMAP* data. From the scaling relations, we show that *WMAP*'s tight bound on $\Omega_b h^2$ is intimately linked to its robust detection of the first and second peaks of the TT spectrum.

Subject headings: cosmic microwave background, cosmology: observations

1. Introduction

WMAP has mapped the cosmic microwave background (CMB) temperature anisotropy over the full sky with unprecedented accuracy (Bennett et al. 2003b). The temperature angular power spectrum (TT, Hinshaw et al. 2003) and the temperature-polarization cross-power spectrum (TE, Kogut et al. 2003) derived from those maps have a number of characteristic features. It is these features, and our ability to predict them, that make the anisotropy such a powerful tool for cosmology. Computer programs like CMBFAST (Seljak & Zaldarriaga 1996) efficiently compute the TT and TE power spectra for a wide variety of cosmological parameters. The model spectra are then compared to the data to deduce the best fit parameters (Spergel et al. 2003). The distinctiveness and accuracy of the measured spectrum determines the degree to which the parameters may be distinguished.

While the parameters of cosmological models are ultimately found by maximizing the likelihood of the data given a model, and the validity of a model is assessed by the goodness of fit (Spergel et al. 2003), this analysis by itself provides no model independent assessment of the features of the angular power spectrum. Both intuition and calculational simplicity fall by the wayside. In this paper we focus on the peaks of the TT and TE spectra. There are four reasons to consider just these particular characteristics. The first is that through an examination of the peaks, one can gain an intuition for how the cosmological parameters are encoded in the TT and TE spectra. The second is that by determining how the peaks depend on cosmological parameters, one may quickly assess how potential systematic errors in the angular power spectra affect some of the cosmological parameters. The third is that alternative models, or additions to the best fit model, may be easily compared to the data simply by checking to see if the alternative reproduces the peak positions and amplitudes. Finally, the peaks serve as a simple check for the sophisticated parameter fitting described in Spergel et al. (2003) and Verde et al. (2003).

The paper is organized as follows. In §2 we give a brief overview of the CMB. In §3 we give *WMAP*'s best fit values for the positions in ℓ-space and amplitudes of the peaks. We then consider, in §4, the cosmological information that comes from the positions and amplitudes of the TT and TE peaks. We interpret the peaks in terms of the best fit model to the full *WMAP* data set (Spergel et al. 2003) and make direct connections to the decoupling epoch. We conclude in §5.

2. Overview

The CMB TT spectrum may be divided into three regions depending on the characteristic angular scale of its features. In each region, a different physical process dominates. The regions correspond to: (a) Angular scales larger than the horizon size at decoupling as observed today. These correspond to $\theta > 2^\circ$ or, equivalently $\ell < \ell_{dec} \approx 90$. The low ℓ portion is termed the Sachs-Wolfe plateau (Sachs & Wolfe 1967). In this region one observes the relatively unprocessed primordial fluctuation spectrum because patches of sky with larger separations could not have been in causal contact at decoupling. (b) The acoustic peak region, $0.^\circ2 < \theta < 2^\circ$ or $90 < \ell < 900$, which is described by the physics of a 3000 K plasma of number density $n_e \approx 300$ cm^{-3} responding to fluctuations in the gravitational potential produced by the dark matter. (c) The Silk damping tail (Silk 1968), $\theta < 0.^\circ2$ or $\ell > 900$, which is produced by diffusion of the photons from the potential fluctuations and the washing out of the net observed fluctuations by the relatively large number of hot and cold regions along the line of sight. The basic framework in which to interpret the temperature anisotropy has been known for over thirty years (Peebles & Yu 1970; Sunyaev & Zel'dovich 1970).

It has long been recognized that the positions and amplitudes of the peaks in the $90 < \ell < 900$ region could be used to constrain the cosmological parameters in a particular model (Doroshkevich et al. 1978; Kamionkowski et al. 1994; Jungman et al. 1996b,a). Previous studies (Scott et al. 1995; Hancock & Rocha 1997; Knox & Page 2000; Weinberg 2000; Cornish 2001; Podariu et al. 2001; Miller et al. 2002; Ödman et al. 2002; Douspis & Ferreira 2002; de Bernardis et al. 2002; Durrer et al. 2003) have steadily increased our understanding of the peaks and their significance.

A summary of pre-*WMAP* determinations of the position and amplitude of the first peak is given in Table 1.

3. Determination of Peak Characteristics

We determine the peaks and troughs with fits of Gaussian and parabolic functions to the data. Through this process, we compress a large data set to eight numbers. Such a compression is similar to specifying the cosmological parameters; though, it is considerably easier to compute and directed more toward the intrinsic characteristics of the data as opposed to a cosmological model.

For the TT spectrum, $\Delta T_\ell^2 \equiv \ell(\ell+1)C_\ell/(2\pi)$, we model the spectrum for $100 < \ell < 700$ as composed of a Gaussian peak, a parabolic trough, and a second parabolic peak independent of any particular cosmological model. Using a parabola to fit the first peak results in a higher χ^2 and systematically underestimates the amplitude. Parabolas are adequate for the other features. The independent parameters are the amplitude and position of each peak and trough, the width

of the first peak, and a continuity parameter. The latera recta[10] of the trough and second peak are derived by constraining the model spectrum to be continuous. The junction between the first peak and the first trough (first trough and second peak) is fixed to be where the first peak (first trough) equals the continuity parameter. In other words, the continuity parameter is the value of the angular power spectrum where the curves meet. There are a total of eight parameters. We denote the positions of the first peak, first trough, and second peak as ℓ_1^{TT}, $\ell_{1.5}^{TT}$, ℓ_2^{TT} respectively. The amplitudes of the first and second peak are $\Delta T^2_{1,TT}$ and $\Delta T^2_{2,TT}$.

The peak parameters are found in three ways: (a) with a direct non-linear fit based on the Levenberg-Marquardt algorithm (Press et al. 1992); (b) with a Markov Chain Monte Carlo (MCMC) (Christensen et al. 2001) of the peak parameters (not the cosmological parameters); and (c) with peak-by-peak fits with a Gaussian fitting function. We have also separately fit the first peak with a Gaussian with additional parameters for kurtosis and skewness. All methods yield consistent results. The values we quote are from the MCMC. All fitting is done with the unbinned angular spectra using the full covariance matrix $\Sigma_{\ell\ell'}$ (Verde et al. 2003). The year one *WMAP* calibration uncertainty is 0.5% which is added in quadruture to the fitted peak amplitude uncertainty. The fit to the TT peak models yields a minimum $\chi^2/\nu = 702/593 = 1.18$. While not as good a fit to the data as a CMBFAST-derived spectrum, the determinations of the peaks are the same for all three methods and are consistent with those of the best fit CMBFAST model.

For the TE spectrum the data between $40 < l < 450$ are modeled as a piecewise-continous composite of a parabolic antipeak and parabolic peak. (We do not fit the reionization region, $\ell < 20$). Each parabola has a latus rectum, height, and position; however, the latus rectum of the antipeak is constrained by the requirement that the antipeak and peak are continuously joined at the zero-crossing. Thus there are just five free parameters. We impose a prior on the latus rectum of the peak to be < 150. The TE Fisher matrix depends on C_ℓ^{TT}, C_ℓ^{TE}, and C_ℓ^{EE}. The TT spectrum is fixed to be a best-fit model, and the small EE contribution is neglected. The best fit model spectrum has $\chi^2/\nu = 504/466 = 1.08$.

The parameters are summarized in Table 2 along with the peak positions determined directly from the MCMC method. These two completely distinct methods yield consistent results. Figure 1 shows the binned TT and TE angular spectrum with the best fit peaks model and the 1σ and 2σ contours for the peak and trough positions. The amplitude of the TT trough and second peak are separated by $> 5\sigma$, leaving no doubt of the existence of the second peak.

Also shown in Table 2 are the peak determinations from the full analysis using just the *WMAP* data (Spergel et al. 2003). The agreement between the two is generally good, most of the values are within 1σ, all are within 1.6σ. This level of discrepancy is expected because the peak fitting and the full analysis weight the data in very different ways.

[10]The *latus rectum* of a conic section is the length of the chord parallel to the directix that passes through the focus. For the parabolic curve $y = y_0 + (x - x_0)^2/w$ the value of the latus rectum is $|w|$.

4. Interpretation of Peaks and Troughs

We now interpret the peak characteristics in terms of a flat adiabatic ΛCDM cosmological model. We focus on the baryon density, $\omega_b = \Omega_b h^2$, the matter density, $\omega_m = \Omega_m h^2$ ($\omega_m = \omega_b + \omega_c$, where ω_c is the cold dark matter component), and the the slope of the primordial power spectrum, n_s. The comparison of the peaks and troughs to the model is made at two levels. At the more general level, we use CMBFAST to derive simple scaling relations and show how the cosmological parameters are encoded in the peak characteristics. The aim is to build an intuition for the connection between the raw data and the deduced parameters. This approach has been championed by Hu et al. (2001); this paper forms the basis for our presentation. The scaling relations hold for a wide range of parameters and may be derived without considering *WMAP* data. However, we optimize them for the best fit *WMAP* parameters (Table 3), so they are as accurate as possible. At a more detailed level, we show that by using the peak values *and* uncertainties with the scaling relations, one obtains constraints and uncertainties on ω_b, ω_m, n_s, and the age of the universe that are consistent with the full analysis (Spergel et al. 2003).

Seljak (1994) and Hu & Sugiyama (1995) showed that the physics of the acoustic peaks may be understood in terms ω_b, ω_m, n_s, τ (the optical depth to when the universe was reionized), and θ_A (the angular scale of the sound horizon at decoupling). Our approach follows that of Hu et al. (2001) in that we consider just the positions of the peaks and the ratios of the peak amplitudes. For $\ell > 40$, the peak ratios are insensitive to the intrinsic amplitude of the CMB spectrum and to τ. The free electrons from reionization at $z \sim 20$ (Kogut et al. 2003) scatter CMB photons, thereby reducing the CMB fluctuations by nearly a constant factor for multipoles $\ell > 40$. (The reionization also increases the TT spectrum at $\ell < 20$ due to Doppler shifts of the scatterers.) We therefore consider just ω_b, ω_m, n_s, and θ_A, in the context of a flat ΛCDM model.

4.1. The Position of the First Peak

The acoustic peaks arise from adiabatic compression of the photon-baryon fluid as it falls into preexisting wells in the gravitational potential. These potential wells are initially the result of fluctuations in some primordial field (e.g., the inflaton field in inflationary cosmology). The wells are enhanced by the dark matter (ω_c), which is able to cluster following matter-radiation equality (z_{eq}, Table 3) because the dark matter, for our purposes, does not scatter off the photons or baryons.

The first peak corresponds to the scale of the mode that has compressed once in the age of the universe at the time that the photons decoupled from the electrons at z_{dec}, some 379^{+8}_{-7} kyr after the Big Bang (Spergel et al. 2003). The characteristic angular scale of the peaks is set by

$$\theta_A \equiv \frac{r_s(z_{dec})}{d_A(z_{dec})}, \tag{1}$$

where r_s is the comoving size of the sound horizon at decoupling and d_A is the comoving angular

size distance to the decoupling surface.

The size of the sound horizon may be computed from the properties of a photon-baryon fluid in an expanding universe. At decoupling it is given by (Hu & Sugiyama 1995, B6):

$$r_s(z_{dec}) = 3997\sqrt{\frac{\omega_\gamma}{\omega_m\omega_b}}\ln\frac{\sqrt{1+R_{dec}}+\sqrt{R_{dec}+R_{eq}}}{1+\sqrt{R_{eq}}} \tag{2}$$

in Mpc, where $R(z) = 3\rho_b(z)/4\rho_\gamma(z)$ with ρ_b the baryon density and ρ_γ the photon density. The redshift at matter-radiation equality is

$$1 + z_{eq} = \frac{5464\,(\omega_m/0.135)}{(T_{\rm CMB}/2.725)^4(1+\rho_\nu/\rho_\gamma)}. \tag{3}$$

The ratio of neutrinos to photons is $\rho_\nu/\rho_\gamma = 0.6851$ (Hannestad & Madsen 1995). Note that $r_s(z_{dec})$ depends only on the physical densities, ω_m and ω_b, and not on h. (We assume $T_{\rm CMB} = 2.725\,{\rm K}$ (Mather et al. 1999) and the number of neutrino species, $N_\nu = 3$.) Also, r_s is independent of the curvature and cosmological constant densities, Ω_k and Ω_Λ, because these are both late acting: at high z the universe evolves as though it is geometrically flat.

The comoving angular size distance[11] to the decoupling surface, d_A, for a flat geometry is

$$d_A = \int_0^{z_{dec}} \frac{H_0^{-1}\,dz}{\sqrt{\Omega_r(1+z)^4+\Omega_m(1+z)^3+\Omega_\Lambda}}, \tag{4}$$

where Ω_r is the current radiation density and $\Omega_\Lambda = 1 - \Omega_m - \Omega_r$ (Peebles 1993). Neither r_s nor d_A depend on n_s. The picture one has is that of measuring the angular size θ_A of a physical meter stick of size r_s near the edge of the observable universe with geodesics of the intervening geometry as encoded in d_A.

The position in ℓ-space of the first peak is intimately linked to θ_A. In fact, in the full analysis (Spergel et al. 2003), θ_A is one of the best determined fit parameters because of its association with the first peak. To make the connection, one defines a characteristic acoustic index, $\ell_A \equiv \pi/\theta_A$. However, ℓ_A is not ℓ_1^{TT} because the potential wells that drive the compression, leading to the large variance at ℓ_1^{TT}, are dynamic: they respond to the matter and radiation that falls into them. Additionally, there is no precise physical relation between an angular scale and an associated ℓ. One calibrates the relation with cosmological models, such as those from CMBFAST, to find a phase factor ϕ_1 that relates the two (Hu et al. 2001). The general relation for all peaks and troughs is

$$\ell_m^{TT} = \ell_A(m - \phi_m), \tag{5}$$

[11] We follow the naming convention of Peebles (1993, 13.29) for d_A. Common alternative names include "proper motion distance" (e.g., Weinberg 1972, 14.4.21), "angular diameter distance" (e.g., Efstathiou & Bond 1999), and "transverse comoving distance" (e.g., Hogg 1999).

where m labels the peak number ($m = 1$ for the first peak, $m = 1.5$ for the first trough, etc.). For a particular curvature density, Ω_k, the ϕ_m depend weakly on ω_b, and ω_m. For example, near the *WMAP* values, changing n_s, ω_b, and ω_m by 10% changes ϕ_1 by 4.6%, 0.5%, and 1.1%, respectively. Because the ϕ_m differ by only $\approx 25\%$ between peaks, ℓ_A may be thought of as the characteristic scale of the peaks in ℓ-space. Effectively, the full analysis solves for the phase factors simultaneously with the other parameters.

The considerations above are quite general and involve a good fraction of the quantities that are of interest to cosmologists. We now show how the *WMAP* peak positions are related to, and in some cases determine, these quantities.

The position of the first peak is an essential ingredient of the mixture of properties that make the CMB such a powerful probe of the geometry of the universe (Kamionkowski et al. 1994; Jungman et al. 1996b). However, the position alone does not determine the geometry. With the full TT spectrum, the quantities that *WMAP* measures particularly well, independent of Ω_k, are ω_m and ω_b because both these quantities affect the spectrum at early times, before geometric effects shift the spectrum. Even if ω_m and ω_b are known, Ω_k and Ω_m (through h) may be traded off one another to give the same θ_A. This is called the "geometric degeneracy" (Bond et al. 1997; Zaldarriaga et al. 1997). The degeneracy is broken with either prior knowledge of h or Ω_m (e.g., Freedman et al. 2001; Bahcall et al. 1999). For *WMAP* if we impose a prior constraint of $h > 0.5$ then $\Omega_k = 0.03 \pm 0.03$; without the prior, $\Omega_k = -0.050^{+0.036}_{-0.039}$ (Spergel et al. 2003). In the following, we take the geometry to be flat and therefore consider the peak positions as a function of ω_b, n_s, and ω_m only.

With known ω_b and ω_m, the acoustic horizon size r_s is particularly well determined. From equation 2 we find $r_s = 143 \pm 4$ Mpc. When n_s is included, we may in addition determine the phases. From the fits in Doran & Lilley (2002) we obtain $\phi_1 = 0.265 \pm 0.006$. The uncertainty is derived from the uncertainties of n_s, ω_b, ω_m, and the quoted accuracy of the fitting function. This combined with the measured position of the first peak at $\ell_1^{TT} = 220.1 \pm 0.8$ gives us an acoustic horizon scale of $\ell_A = 300 \pm 3$. And, from ℓ_A we find that $\theta_A = 0.601 \pm 0.005^\circ$. In other words, we know the angular and physical sizes of structures on the decouping surface very well. From equation 1, we solve for the angular size distance and find that $d_A = 13.7 \pm 0.4\,\mathrm{Gpc}$. If we had naively tried to compute d_A from h and Ω_m and their uncertainties directly from equation 4, the resulting uncertainty would have been larger. This, though, is not the correct procedure because the h and Ω_m deduced from the CMB are correlated as shown in Figure 2.

The interplay between measuring the peak position, and thus d_A, and measuring ω_m is at the root of *WMAP*'s ability to determine Ω_m and h separately (Bond et al. 1994; Efstathiou & Bond 1999). In particular, Percival et al. (2002) show that θ_A, which depends primarily on the first peak position, is the same along a line of constant $\Omega_m h^{3.4}$. In other words, this is how Ω_m and h scale to keep θ_A constant. In Figure 2 we show the constraint from the measured first peak position. For each coordinate pair in the plane, we compute ℓ_1^{TT} from equations 1, 2, 4, and 5

and then assign the pair a likelihood derived from the measured distribution of $\ell_1^{TT} = 220.1 \pm 0.8$. (We set $\omega_b = 0.023$ for the calculation as discussed below.) The figure also shows the constraints from ω_m and the likelihood contours from the full *WMAP* likelihood analysis. It is evident that the departure from a fixed $\Omega_m h^2$ dependence in θ_A enables separating Ω_m and h. The separation is by no means complete and constitutes one of the largest parameter degeneracy for *WMAP*; it precludes determining $\Omega_\Lambda = 1 - \Omega_m$ to high precision with CMB data alone. The independent determination of Ω_m and h will improve with time as the uncertainty on ω_m decreases. Fortunately, galaxy surveys are sensitive to $\Omega_m h$ which breaks the degeneracy when the data sets are combined (Spergel et al. 2003).

It is fortuitous that in a flat geometry the position of the first peak is directly correlated with the age of the universe (Knox et al. 2001; Hu et al. 2001). This is seen most easily in the $\Omega_m - h$ plane in Figure 2. With $w = -1$, the age depends only on the expansion time scale h^{-1} and Ω_m and is given by

$$t_0 = 6.52 h^{-1} (1 - \Omega_m)^{-1/2} \ln\left(\frac{1 + \sqrt{1 - \Omega_m}}{\sqrt{\Omega_m}}\right) \text{ [Gyr]} \tag{6}$$

(Carroll et al. 1992). We show the isochrons for 12 Gyr through 16 Gyr. One observes that they overlap considerably with the position constraint and the degeneracy lines from equation 4. For reasonable values of Ω_m, the age is seen to be in the neighborhood of 13.6 Gyr. The full analysis (Spergel et al. 2003) gives $t_0 = 13.6 \pm 0.2$ Gyr for $w = -1$. Changing ω_b changes the position constraint through changes in r_s and ϕ_1. If ω_b is increased from 0.024 to 0.025 (1σ), the position constraint line shifts by $< \sigma/2$, indicating that the plot is not particularly sensitive to changes in ω_b.

To summarize this section, we have shown how the position of the first peak is related to the cosmological parameters. Traditionally, one has used equation 5, the weak dependence of ϕ on ω_b and ω_m, $n_s \approx 1$ and the measured position of the first peak to deduce flatness. Instead, we assumed flatness and use *WMAP*'s values of n_s, ω_b and ω_m, to deduce a precise relation for the acoustic scale, ℓ_A. We then showed how one of the largest parameter degeneracy in the CMB data could be understood in terms trading off h and Ω_m in θ_A. Finally, we showed that *WMAP*'s measure of the age of the universe is largely a function of *WMAP*'s identification of the position of the first peak.

4.2. The Amplitude of the First Peak

The scaling of the amplitude of the first peak with ω_b and ω_m has a straightforward interpretation. However, unlike the position, the amplitude itself has a complicated dependence on the cosmological parameters (Efstathiou & Bond 1999; Hu et al. 2001). We defer discussing the ω_b scaling until after §4.3 and consider here just the ω_m scaling.

Increasing ω_m decreases the first peak height. When the universe is radiation dominated at $z > z_{eq}$ and the photon-baryon fluid compresses in a gravitational potential well, the depth of the

well is decreased due to the additional mass loading of the fluid. As a result, the compressed fluid can expand more easily because it sees a shallower potential. The process is termed "radiation driving" (Hu & Sugiyama 1995; Hu & Dodelson 2002) and enhances the oscillations. (In addition, a shallower potential well means that the photons are redshifted less as they climb out enhancing the effect further.) The effect remains important through recombination. Increasing ω_m, while holding all else but Ω_Λ constant, moves the epoch of matter-radiation equality to higher redshifts without significantly affecting z_{dec}. This gives the dark matter more time to develop the potential wells into which the photon-baryon fluid falls. With better defined potential wells, the compressed photon-baryon fluid has less of an effect on them, thereby reducing the effects of radiation driving. As a consequence, increasing ω_m decreases the amplitude of the fluctuations for all the acoustic peaks.

4.3. Additional TT Peaks and Troughs

There is a pronounced second peak in the *WMAP* TT spectrum at a height $> 5\sigma$ above the first trough. The peak arises from the rarefaction phase of an acoustic wave. In broad terms (Hu & Dodelson 2002), in the same conformal time that it takes the plasma to compress over the acoustic horizon, an acoustic wave with half the wavelength (twice the ℓ) of the first peak can compress and rarify. Likewise, a compressional third peak is expected at the second harmonic of the first peak and a rarefaction fourth peak is expected at the third harmonic of the first peak. This set of peaks, the first two of which *WMAP* clearly sees, shows that the photon-baryon fluid underwent acoustic oscillations.

The position of the first trough, and the second and subsequent peaks is predicted from the acoustic scale and phase shifts. From equation (5) and the values in Table 3, one predicts $\ell_{1.5}^{TT} = 409 \pm 4$, $\ell_2^{TT} = 533 \pm 5$, and $\ell_3^{TT} = 809 \pm 7$. The first two of these values agree with those found from the peak fits to within the measurement uncertainty as shown in Table 2.

The amplitude of the second peak depends on many of the same parameters as the amplitude of the first. Its most distinctive feature, though, is that increasing ω_b *decreases* its height. The reason is that as one increases the baryon density one increases the inertia in the photon-baryon fluid. When compared to the lower ω_b case, the compressions are deeper and the rarefactions not as pronounced. Thus, the compressional peaks are hotter (first and third) and the rarefaction peaks (second and fourth) are cooler.

Following Hu et al. (2001) we characterize the amplitude of second peak as a ratio to the amplitude of the first peak, H_2^{TT}. The ratio is insensitive to the reionization optical depth and to the overall amplitude of the spectrum since they simply scale the amplitudes of both peaks. It depends on just ω_b, ω_m, and n_s. The dependence on ω_m is relatively weak, since to a first approximation it too just scales the peak amplitudes as discussed above. The dependence on n_s simply comes from the overall slope of the CMB angular spectrum. Increasing n_s increases the

height of the second peak relative to the first. The following function is derived from fitting to a grid of CMBFAST spectra. It gives the ratio of the peak amplitudes to 2% accuracy for 50% variations in the parameters:

$$H_2^{TT} \equiv \left(\frac{\Delta T_2^{\rm TT}}{\Delta T_1^{\rm TT}}\right)^2 = 0.0264\,\omega_b^{-0.762}(2.42)^{n_s-1} \times e^{-0.476\ln(25.5\omega_b+1.84\omega_m)^2} \quad (7)$$

the parameter dependences are

$$\frac{\Delta H_2^{TT}}{H_2^{TT}} = 0.88\Delta n_s - 0.67\frac{\Delta\omega_b}{\omega_b} + 0.039\frac{\Delta\omega_m}{\omega_m}. \quad (8)$$

Thus a 1% increase in both ω_b and ω_m with n_s fixed reduces the height of the second peak relative to the first by 0.63%.

For the *WMAP* data, $H_2^{TT} = 0.426 \pm 0.015$. In Figure 3 we show the constraints from H_2^{TT} for $\omega_m = 0.14$. The contour lines correspond to the full analysis (Spergel et al. 2003). One sees that the two analyses are consistent, though the error from just considering H_2^{TT} is larger. However, it is clear that the uncertainty in H_2^{TT} for ω_b at fixed n_s and ω_m leads to nearly the same uncertainty as deduced from the full analysis. Thus, we may interpret *WMAP*'s ability to determine ω_b as coming primarily from the precise measurement of the ratio of the first two peaks. The first two terms on the right side of the above equation, as shown in Figure 3, also quantify the $\omega_b - n_s$ degeneracy (Spergel et al. 2003).

The height of the third peak *increases* as ω_b increases, as discussed above, and increasing ω_m decreases its height. Thus the ratio to the first peak is not as distinctive as for the second peak in terms of ω_b and ω_m but the long ℓ baseline makes the ratio more sensitive to n_s. Hu et al. (2001) give:

$$H_3^{TT} \equiv \left(\frac{\Delta T_3^{\rm TT}}{\Delta T_1^{\rm TT}}\right)^2 = \frac{2.17\omega_m^{0.59}\,3.6^{n_s-1}}{[1+(\omega_b/0.044)^2][1+1.63(1-\omega_b/0.071)\omega_m]} \quad (9)$$

with parameter dependencies

$$\frac{\Delta H_3^{TT}}{H_3^{TT}} = 1.28\Delta n_s - 0.39\frac{\Delta\omega_b}{\omega_b} + 0.46\frac{\Delta\omega_m}{\omega_m}. \quad (10)$$

With n_s fixed, increasing ω_b and ω_m by 1% increases the height of the third peak relative to the first by only 0.07%. Measuring the third peak helps mostly in measuring n_s, thereby breaking the $\omega_b - n_s$ degeneracy shown in the left side of Figure 3. For *WMAP* parameters, equation 10 is accurate to 1%.

WMAP does not yet clearly measure the third peak. For its height, we use the value of the Wang et al. (2002) compilation because it is the most recent and includes calibration error. At $l = 801$, $(\Delta T_\ell^{\rm TT})^2 = 2322 \pm 440\,\mu{\rm K}^2$. Though not quite at the peak, the value is sufficient. With *WMAP*'s first peak, $H_3^{TT} = 0.42 \pm 0.08$.

4.4. The Temperature-Polarization peaks

The E-mode polarization in the CMB arises from Thompson scattering of a quadrupolar radiation pattern at the surface of last scattering. At decoupling, the quadrupolar pattern is produced by velocity gradients in the plasma and is correlated with the temperature anisotropy (Bond & Efstathiou 1984; Coulson et al. 1994). In rough terms, because it is velocity dependent, the temperature-polarization correlation traces the derivative of the temperature spectrum. For a given TT spectrum, the (non-reionized) TE and EE spectra are predicted. Thus, their observation confirms that the cosmological model is correct but in so far as they are predicted for $\ell > 40$, they contain little additional information about the parameters. By contrast, the TE polarization signal at $\ell < 20$ (Kogut et al. 2003), produced by reionized electrons scattering the local $z_r \sim 20$ CMB quadrupole, breaks a number of parameter degeneracies and considerably enhances the ability to extract the cosmic parameters.

From parameterizing the output of CMBFAST, we find that the ratio of the first TE antipeak to the second TE peak is given by

$$H_2^{\rm TE} \equiv -\left(\frac{\Delta T_1^{\rm TE}}{\Delta T_2^{\rm TE}}\right)^2 = 0.706\,\omega_m^{0.349}(0.518)^{n_s-1} \times e^{0.195\ln(33.6\omega_b+5.94\omega_m)^2}. \quad (11)$$

The parameter dependencies are

$$\frac{\Delta H_2^{TE}}{H_2^{TE}} = -0.66\Delta n_s + 0.095\frac{\Delta\omega_b}{\omega_b} + 0.45\frac{\Delta\omega_m}{\omega_m}. \quad (12)$$

The sign preceding Δn_s is opposite to that in the case of the TT peaks since we are considering the ratio of the first antipeak (low ℓ) to the second peak (high ℓ), whereas in the case of the TT peaks we were considering the second peak (high ℓ) to the first peak (low ℓ). Here, increasing ω_m *increases* the contrast between the TE peak and antipeak. This occurs because increasing ω_m leads to deeper potential wells at decoupling. In turn, this produces higher velocities and thus an enhanced polarization signal. From the data we find $H_2^{\rm TE} = 0.33 \pm 0.10$.

4.5. Combined Peak Constraints

We now use the scaling relations just presented in a flat model with the scalar index limited to $n_s = 0.99$. This simplified minimal model leads to a greater intuition for assessing the peaks'

role in determining the cosmological parameters. The constraints from H_2^{TT} and H_3^{TT} are shown in Figure 3. We see that H_2^{TT} determines ω_b for most values of the dark matter and that $\omega_b < 0.029$ (2σ) regardless of the amount of dark matter. The width of the swath is about twice that of the formal error, again indicating that more in the spectrum than just H_2^{TT} constrains ω_b.

The constraints from H_2^{TE} and H_3^{TT} are almost orthogonal to the H_2^{TT} constraint but their uncertainty bands are wide. This shows us that the *WMAP* value for ω_c (or ω_m) is not being driven specifically by the peak ratios. Rather, the constraint comes from the amplitude of the whole spectrum. The degeneracy with τ is broken by the TE detection of reionization and the degeneracy with the overall amplitude is broken because ω_m affects primarily the acoustic peak region more than the low ℓ part of the spectrum.

5. Discussion

We have focused on the dominant acoustic features in the *WMAP* spectrum, but there are other features as well. Notable by its absence is a trough in the TT spectrum at $\ell \approx 10$ due to the increase in fluctuation power near $\ell = 2$ from the integrated Sachs-Wolfe effect in a Λ-dominated universe. This feature is largely obscured by cosmic variance. For *WMAP* though, there is very little power at low ℓ and the correlations with $\theta > 60^\circ$ are unusually small (Bennett et al. 2003a). The lack of even a hint of an upturn at low ℓ, in the context of ΛCDM models, is surprising. (However, *COBE* also found no evidence for such an upturn). This departure from the model constitutes a small (though possibly important) fraction of the total fluctuation power and does not cast doubt on the interpretation of the $\ell > 40$ spectrum.

At $\ell \approx 40$ and $\ell \approx 210$, for example, there are excursions from a smooth spectrum that are somewhat larger than expected statistically. While intriguing, they may result from a combination of cosmic variance, subdominant astrophysical processes, and small effects from approximations made for the year one data analysis (Hinshaw et al. 2003). At present, we consider them interesting but do not attach cosmological significance to them (e.g., Peiris et al. 2003; Bose & Grishchuk 2002). More integration time and more detailed analyses are needed to understand how they should be interpreted.

In summary, the characteristics of the peaks of the *WMAP* angular power spectra may be robustly extracted from the data. The second TT peak is seen with high accuracy; the TE antipeak and peak have been observed for the first time. In the context of a flat adiabatic ΛCDM model, which fits the *WMAP* data well, we report the characteristics of the decoupling surface. By considering a reduced parameter space, we show how the position of the first peak leads to *WMAP*'s tight determination of the age of the universe and how ω_b is determined primarily from the amplitude ratio of the first to second TT peak. The determination of ω_m comes from considering the full data set and is not attributable to any particular peak ratio.

LP is grateful to Viatcheslav Mukhanov for helpful discussions on the parameter dependences of the peaks during his year at Princeton and to Alessandro Melchiorri for discussing his work on peaks prior to publication. LP especially thanks Toby Marriage for many enlightening discussions on the first peak. We also thank Eiichiro Komatsu, Licia Verde, Will Sutherland, and an anonymous reviewer for comments that improved this paper. The *WMAP* mission is made possible by the support of the Office of Space Sciences at NASA Headquarters and by the hard and capable work of scores of scientists, engineers, technicians, machinists, data analysts, budget analysts, managers, administrative staff, and reviewers.

REFERENCES

Bahcall, N. A., Ostriker, J. P., Perlmutter, S., & Steinhardt, P. J. 1999, Science, 284, 1481

Bennett, C. L., et al. 2003a, ApJ, submitted

—. 2003b, ApJ, 583, 1

Benoit, A. et al. 2003, A&A, submitted (astro-ph/0210305)

Bond, J. R., Crittenden, R., Davis, R. L., Efstathiou, G., & Steinhardt, P. J. 1994, Phys. Rev. Lett., 72, 13

Bond, J. R. & Efstathiou, G. 1984, ApJ, 285, L45

Bond, J. R., Efstathiou, G., & Tegmark, M. 1997, MNRAS, 291, L33

Bose, S. & Grishchuk, L. P. 2002, Phys. Rev. D, 66, 43529

Carroll, S. M., Press, W. H., & Turner, E. L. 1992, ARA&A, 30, 499

Christensen, N., Meyer, R., Knox, L., & Luey, B. 2001, Classical and Quantum Gravity, 18, 2677

Cornish, N. J. 2001, Phys. Rev. D, 63, 27302

Coulson, D., Crittenden, R. G., & Turok, N. G. 1994, Phys. Rev. Lett., 73, 2390

de Bernardis, P., et al. 2002, ApJ, 564, 559

Doran, M. & Lilley, M. 2002, MNRAS, 330, 965

Doroshkevich, A. G., Zel'dovich, Y. B., & Sunyaev, R. A. 1978, Soviet Astronomy, 22, 523

Douspis, M. & Ferreira, P. 2002, Phys. Rev. D, 65, 087302

Durrer, R., Novosyadlyj, B., & Apunevych, S. 2003, ApJ, 583, 33

Efstathiou, G. & Bond, J. R. 1999, MNRAS, 304, 75

Freedman, W. L., et al. 2001, ApJ, 553, 47

Grainge, K. et al. 2003, MNRAS, in press (astro-ph/0212495)

Halverson, N. W., et al. 2002, ApJ, 568, 38

Hancock, S. & Rocha, G. 1997, in Microwave Background Anisotropies, 179

Hannestad, S. & Madsen, J. 1995, Phys. Rev. D, 52, 1764

Hinshaw, G. F. et al. 2003, ApJ, submitted

Hogg, D. W. 1999, Distance measures in cosmology, astro-ph/9905116

Hu, W. & Dodelson, S. 2002, ARA&A, 40, 171

Hu, W., Fukugita, M., Zaldarriaga, M., & Tegmark, M. 2001, ApJ, 549, 669

Hu, W. & Sugiyama, N. 1995, ApJ, 444, 489

—. 1996, ApJ, 471, 542

Jungman, G., Kamionkowski, M., Kosowsky, A., & Spergel, D. N. 1996a, Phys. Rev. D, 54, 1332

—. 1996b, Physical Review Letters, 76, 1007

Kamionkowski, M., Spergel, D. N., & Sugiyama, N. 1994, ApJ, 426, L57

Knox, L., Christensen, N., & Skordis, C. 2001, ApJ, 563, L95

Knox, L. & Page, L. 2000, Phys. Rev. Lett., 85, 1366

Kogut, A. et al. 2003, ApJ, submitted

Lee, A. T. et al. 2001, ApJ, 561, L1

Mather, J. C., Fixsen, D. J., Shafer, R. A., Mosier, C., & Wilkinson, D. T. 1999, ApJ, 512, 511

Mauskopf, P. D., et al. 2000, ApJ, 536, L59

Miller, A. D. et al. 1999, ApJ, 524, L1

Miller, C. J., Nichol, R. C., Genovese, C., & Wasserman, L. 2002, ApJ, 565, L67

Ödman, C. J., Melchiorri, A., Hobson, M. P., & Lasenby, A. N. 2002, Phys. Rev. D, submitted (astro-ph/0207286)

Page, L. et al. 2003, ApJ, 585, in press

Peebles, P. J. E. 1993, Principles of Physical Cosmology (Princeton, NJ: Princeton University Press)

Peebles, P. J. E. & Yu, J. T. 1970, ApJ, 162, 815

Peiris, H. et al. 2003, ApJ, submitted

Percival, W. J., et al. 2002, MNRAS, 337, 1068

Podariu, S., Souradeep, T., Gott, J. R. I., Ratra, B., & Vogeley, M. S. 2001, ApJ, 559, 9

Press, W. H., Teukolsky, S. A., Vetterling, W. T., & Flannery, B. P. 1992, Numerical Recipes in C, 2nd edn. (Cambridge, UK: Cambridge University Press)

Ruhl, J. E. et al. 2003, ApJ, submitted (astro-ph/0212229)

Sachs, R. K. & Wolfe, A. M. 1967, ApJ, 147, 73

Scott, D., Silk, J., & White, M. 1995, Science, 268, 829

Seljak, U. 1994, ApJ, 435, L87

Seljak, U. & Zaldarriaga, M. 1996, ApJ, 469, 437

Silk, J. 1968, ApJ, 151, 459

Spergel, D. N. et al. 2003, ApJ, submitted

Sunyaev, R. A. & Zel'dovich, Y. B. 1970, Ap&SS, 7, 3

Verde, L. et al. 2003, ApJ, submitted

Wang, L., Caldwell, R. R., Ostriker, J. P., & Steinhardt, P. J. 2000, ApJ, 530, 17

Wang, X., Tegmark, M., Jain, B., & Zaldarriaga, M. 2002, Phys. Rev. D, submitted (astro-ph/0212417)

Weinberg, S. 1972, Gravitation and Cosmology (New York, NY: John Wiley)

Weinberg, S. 2000, Phys. Rev. D, 62, 127302

Zaldarriaga, M., Spergel, D. N., & Seljak, U. 1997, ApJ, 488, 1

This preprint was prepared with the AAS LaTeX macros v5.0.

Table 1. Previous Measurements of the First Peak

Experiment	ℓ_1^{TT}	$\Delta T_{1,TT}$ [μK]	Cal. error	ℓ range	Reference
TOCO	207^{+15}_{-12}	87^{+9}_{-8}	8%	$60 < \ell < 410$	Miller et al. (1999)
BOOMERANG-NA	207^{+26}_{-20}	$69.6^{+9.7}_{-8.4}$	8%	$50 < \ell < 410$	Mauskopf et al. (2000)
MAXIMA	236 ± 14	$70.0^{+5.3}_{-5.3}$	4%	$75 < \ell < 385$	Lee et al. (2001)
DASI	199^{+15}_{-18}	71.9 ± 4.4	4%	$110 < \ell < 380$	Halverson et al. (2002)
VSA	236^{+20}_{-26}	73.9 ± 6.8	3.5%	$140 < \ell < 420$	Grainge et al. (2003)
BOOMERANG	219 ± 5	$73.8^{+8.5}_{-7.0}$	10%	$100 < \ell < 410$	Ruhl et al. (2003)
ARCHEOPS	220^{+7}_{-6}	$70.2^{+5.7}_{-4.9}$	7%	$18 < \ell < 330$	Benoit et al. (2003)
WMAP	220.1 ± 0.8	74.7 ± 0.5	0.5%	$100 < \ell < 350$	This paper

Note. — All values come from fitting a Gaussian shape to just the first peak of the data set specified, and include calibration error. Each data set is considered on its own, without the *COBE*/DMR data, and so a direct comparison between experiments may be made. The best fit position depends somewhat on the fitting function so the values from different analyses yield different results (e.g., Knox & Page 2000; Durrer et al. 2003; Ödman et al. 2002; Grainge et al. 2003). The TOCO, VSA, and BOOMERANG-NA experiments were calibrated with Jupiter. The TOCO and VSA experiments are most affected because of they operate at 30-150 GHz and 35 GHz respectively. With the new calibration of Jupiter (Page et al. 2003), the peak values above will be reduced $\approx 5\%$. The weighted peak amplitude is 71.7 ± 2.4 μK and the weighted peak position is 218.8 ± 3.5 in good agreement with *WMAP*. In a separate analysis based on different assumptions, Bond reports $\ell_1^{TT} = 222 \pm 3$ (private communication). This was also the value preferred by a concordance model (Wang et al. 2000) that predated all the experiments of the new millennium. Note that *WMAP*'s values for the position and amplitude are both more than four times more precise than all the listed measurements combined.

Table 2. *WMAP* Peak and Trough Amplitudes and Positions

Quantity	Symbol	ℓ	ΔT_ℓ [μK]	ΔT_ℓ^2 [μK^2]	FULL ℓ	FULL ΔT_ℓ^2 [μK^2]
First TT Peak	ℓ_1^{TT}	220.1 ± 0.8	74.7 ± 0.5	5583 ± 73	219.8 ± 0.9	5617 ± 72
First TT Trough	$\ell_{1.5}^{TT}$	411.7 ± 3.5	41.0 ± 0.5	1679 ± 43	410.0 ± 1.6	1647 ± 33
Second TT Peak	ℓ_2^{TT}	546 ± 10	48.8 ± 0.9	2381 ± 83	535 ± 2	2523 ± 49
First TE Antipeak	ℓ_1^{TE}	137 ± 9	$\cdots$	-35 ± 9	151.2 ± 1.4	-45 ± 2
Second TE Peak	ℓ_2^{TE}	329 ± 19	$\cdots$	105 ± 18	308.5 ± 1.3	117 ± 2

Note. — The values and uncertainties are the maximum and width of the a posteriori distribution of the likelihood assuming a uniform prior. The uncertainties include calibration uncertainty and cosmic variance. The FULL values are derived from the full CMBFAST-based likelihood analysis using just the *WMAP* data (Spergel et al. 2003). The FULL method yields consistent results. Recall that the FULL chains are sensitive to the combined TT and TE spectra and not just the individual peak regions. Numerical errors in CMBFAST will increase the uncertainties, but should not bias the results.

Table 3. *WMAP* Cosmological Parameters for the Peaks Analysis

Quantity	Symbol	Value	
Physical baryon density	ω_b	0.024 ± 0.001	
Physical mass density	ω_m	0.14 ± 0.02	INPUT
Scalar index	n_s	0.99 ± 0.04	
First TT peak phase shift	ϕ_1	0.265 ± 0.006	
First TT trough phase shift	$\phi_{1.5}$	0.133 ± 0.007	
Second TT peak phase shift	ϕ_2	0.219 ± 0.008	DERIVED
Third TT peak phase shift	ϕ_3	0.299 ± 0.005	FROM
Redshift at decoupling	z_{dec}	1088^{+1}_{-2}	INPUT
Redshift at matter radiation equality	z_{eq}	3213^{+339}_{-328}	
Comoving acoustic horizon size at decoupling (Mpc)	r_s	143 ± 4	
Acoustic scale	l_A	300 ± 3	DERIVED FROM
Comoving angular size distance to decoupling (Gpc)	d_A	13.7 ± 0.4	INPUT + PEAKS

Note. — The cosmological parameters in the top section are derived from just the *WMAP* data assuming a flat ΛCDM model (Spergel et al. 2003). The quantities in the middle section are derived from the cosmological parameters in the top section. The quantities in bottom section are calculated using the middle quantities and the measured position of the first peak. The quantity z_{dec} which we use corresponds to the location of the maximum of the visibility function in CMBFAST. The quantity computed using Hu & Sugiyama (1996) corresponds to $\tau(z_{dec}) = 1$ and is 1090 ± 2.

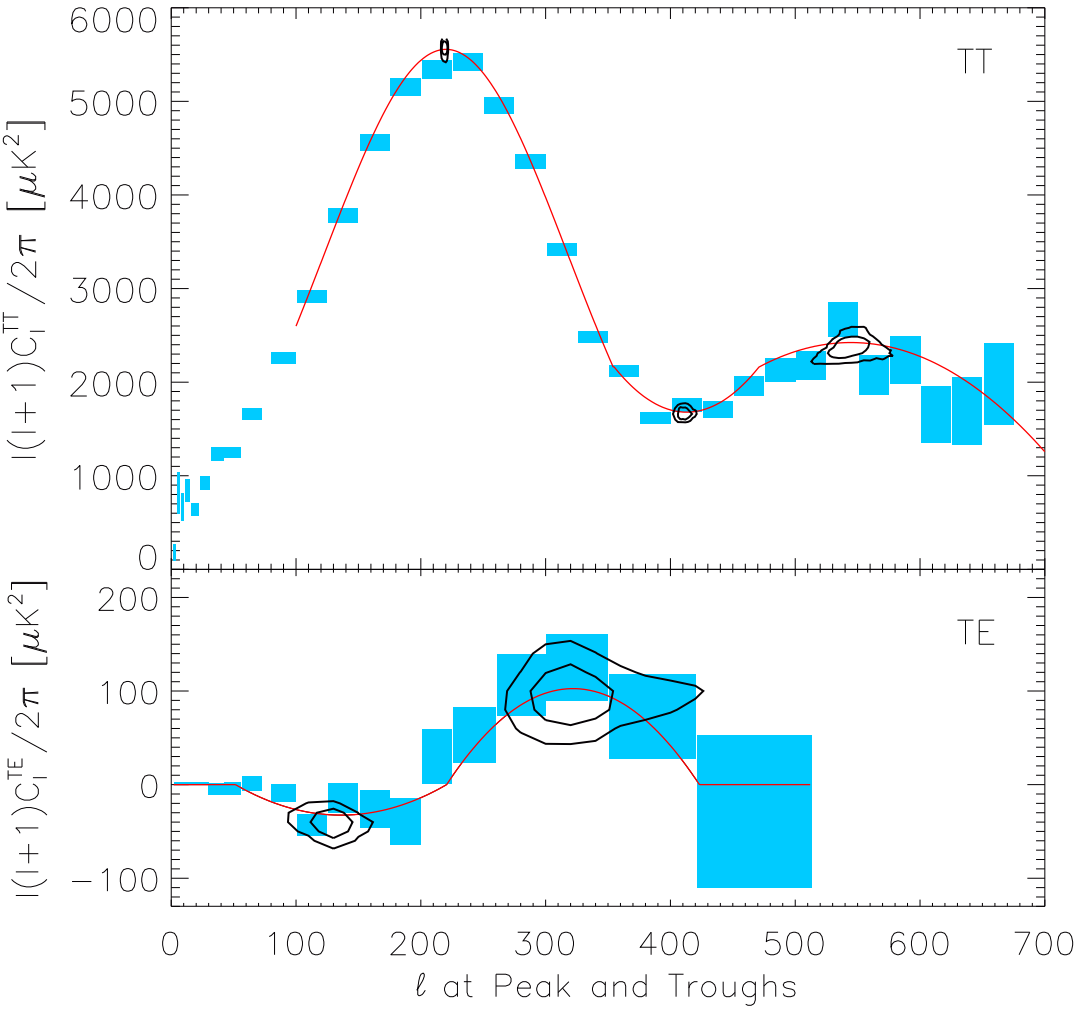

Fig. 1.— The binned *WMAP* data is shown in blue, the maximum likelihood peak model from the peak fitting functions in red, and the uncertainty contours in black. The top panel shows the TT angular power spectrum. The bottom panel shows the TE angular cross-power spectrum. For each peak or trough, the contours from the MCMC chains are multiplied by a uniform prior and so they are equal to contours of the a posteriori likelihood of the data given the model. The contours are drawn at $\Delta\chi^2 = 2.3$ and 6.18 corresponding to 1σ and 2σ.

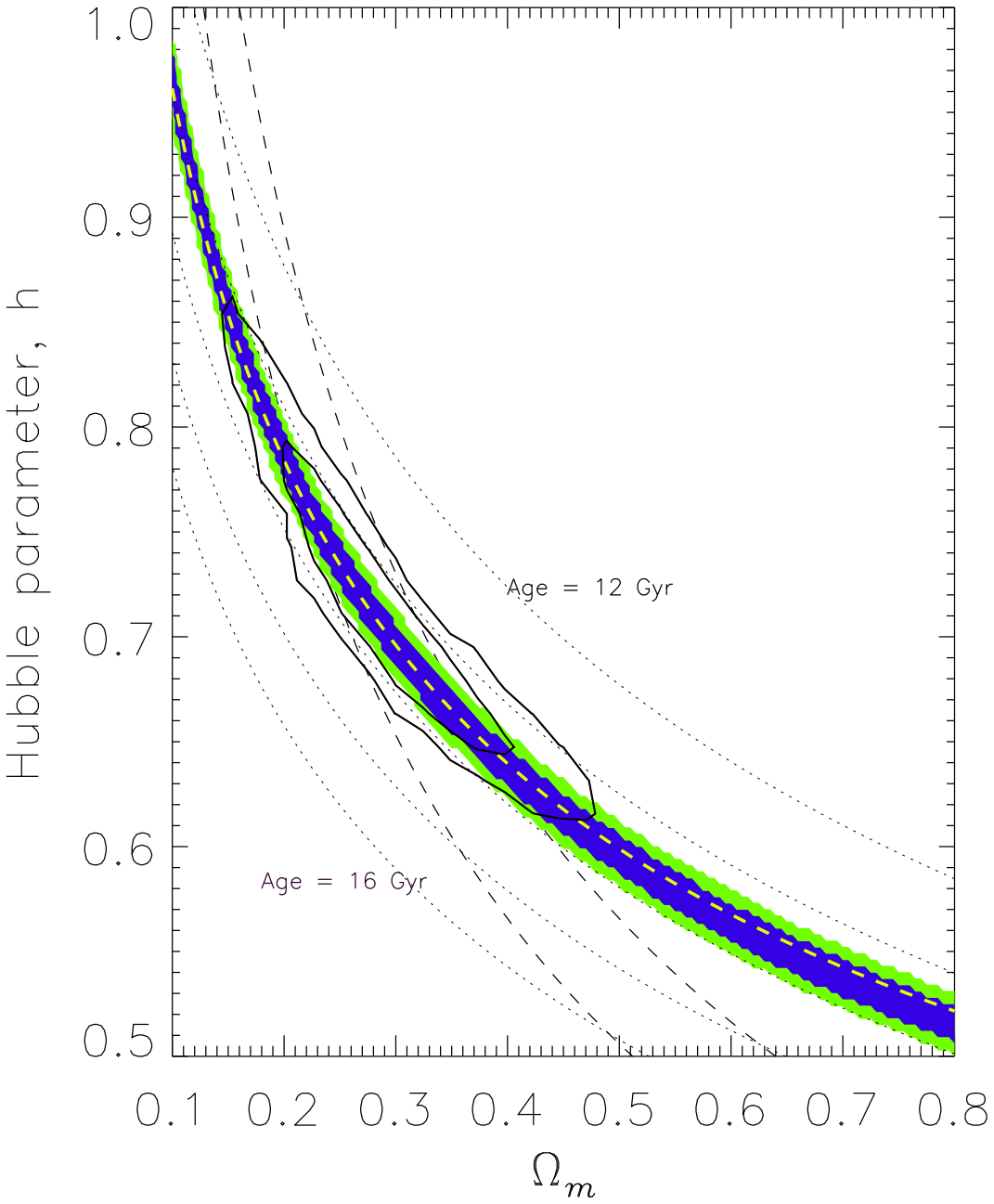

Fig. 2.— The *WMAP* data in the $\Omega_m - h$ plane. The thick solid contours in black are at $\Delta\chi^2 = -2.3, -6.18$ (1σ, 2σ) of the marginalized likelihood from the full analysis (Spergel et al. 2003). The filled region is the constraint from the position of the first peak, with $\omega_b = 0.023$ fixed. In effect, it shows how Ω_m and h must be related to match the observed position of the first peak in a flat geometry, or equivalently to match the measured values of θ_A. Blue shows the 1σ region and green shows the 2σ region. The dotted lines are isochrons separated by 1 Gyr. It is clear that the *WMAP* data pick out 13.6 Gyr for the age of the universe in the flat, $w = -1$ case. The dashed lines show the 1σ limits on ω_m. The dashed yellow line shows $\Omega_m h^{3.4} = \text{const}$.

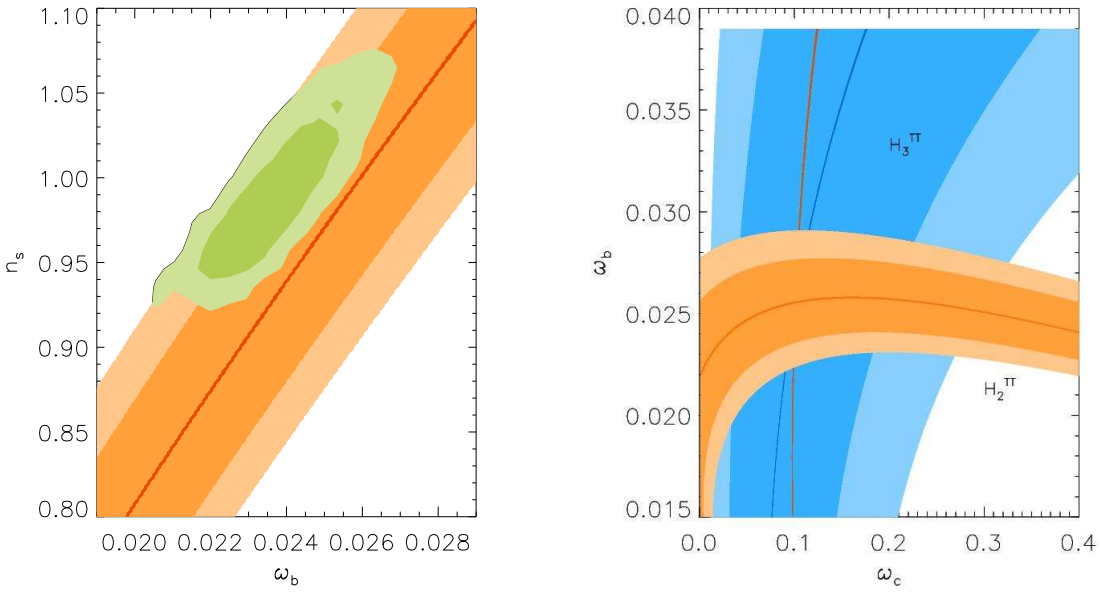

Fig. 3.— Left: Parameter restrictions from H_2^{TT} in the $\omega_b - n_s$ plane. The orange swath is the 1σ band corresponding to $H_2^{TT} = 0.426 \pm 0.015$ with $\omega_m = 0.14$. The swath is broadened if one includes the uncertainty in ω_m. The light orange swath is 2σ. The solid line in the middle of the swath is for $\Delta H_2^{TT} = \Delta\omega_m = 0$. The green contours are from the full analysis of just the *WMAP* data and are thus more restrictive. Right: The constraints in the $\omega_b - \omega_c$ plane from the peak ratios in a flat geometry with $n_s = 0.99$. The dark shaded regions in each swath are the 1σ allowed range; the light shaded regions show the 2σ range. Orange is for $H_2^{TT} = 0.426 \pm 0.015$, blue is for $H_3^{TT} = 0.42 \pm 0.08$, and red is for $H_2^{TE} = 0.33 \pm 0.10$. The uncertainty band for H_2^{TE} is not shown as it is broader than the H_3^{TT} swath. The heavier central lines correspond to $\Delta H_2^{TT} = 0$, $\Delta H_3^{TT} = 0$, and $\Delta H_2^{TE} = 0$, each with $\Delta n_s = 0$. As the mission progresses, all uncertainties will shrink.